

# HyperAlign: Hyperbolic Entailment Cones for Adaptive Text-to-Image Alignment Assessment

Wenzhi Chen<sup>1</sup>, Bo Hu<sup>1</sup>, Leida Li<sup>2</sup>, Lihuo He<sup>2</sup>, Wen Lu<sup>2</sup> and Xinbo Gao<sup>1,2\*</sup>

<sup>1</sup>Chongqing University of Posts and Telecommunications

<sup>2</sup>Xidian University

d250201005@stu.cqupt.edu.cn, hubo90@cqupt.edu.cn, ldli@xidian.edu.cn, {lhhe, luwen}@mail.xidian.edu.cn, gaoxb@cqupt.edu.cn

## Abstract

With the rapid development of text-to-image generation technology, accurately assessing the alignment between generated images and text prompts has become a critical challenge. Existing methods rely on Euclidean space metrics, neglecting the structured nature of semantic alignment, while lacking adaptive capabilities for different samples. To address these limitations, we propose HyperAlign, an adaptive text-to-image alignment assessment framework based on hyperbolic entailment geometry. First, we extract Euclidean features using CLIP and map them to hyperbolic space. Second, we design a dynamic-supervision entailment modeling mechanism that transforms discrete entailment logic into continuous geometric structure supervision. Finally, we propose an adaptive modulation regressor that utilizes hyperbolic geometric features to generate sample-level modulation parameters, adaptively calibrating Euclidean cosine similarity to predict the final score. HyperAlign achieves highly competitive performance on both single database evaluation and cross-database generalization tasks, fully validating the effectiveness of hyperbolic geometric modeling for image-text alignment assessment.

## 1 Introduction

In recent years, Text-to-Image (T2I) generation models such as Stable Diffusion [Rombach *et al.*, 2022], DALL-E [Ramesh *et al.*, 2021], and Midjourney have achieved breakthrough progress, fundamentally reshaping production paradigms in domains including media creation, artistic design, and advertising. However, the alignment degree between generated images and text prompts varies considerably. Unlike Natural Scene Image Quality Assessment (NS-IQA), users primarily focus on the degree of content alignment between generated images and input text prompts. Only when images faithfully reflect user intentions do considerations of aesthetic appeal and realism become meaningful. Therefore,

establishing automated, high-precision Text-to-Image Alignment Assessment (T2IAA) methods not only provides alignment feedback to users but also serves as reward models to guide reinforcement learning optimization of generative models [Hu *et al.*, 2025], holding significant research value.

Traditional NS-IQA methods, ranging from handcrafted methods [Mittal *et al.*, 2012; Mittal *et al.*, 2013] to deep learning methods [Zhang *et al.*, 2020], have produced numerous classical methods over decades of development. Although these methods demonstrate considerable effectiveness when assessing natural image quality, they cannot understand cross-modal semantic mappings and thus fail to transfer effectively to T2IAA tasks. Existing T2IAA research primarily relies on large-scale vision-language pre-trained models like CLIP [Radford *et al.*, 2021] to map images and text into the same feature space, generally following two strategies: one is similarity-based metrics, such as AMFF-Net [Zhou *et al.*, 2024] and CIA-Net [Zhou *et al.*, 2025], which directly map cosine similarity to alignment scores; the other is learning-based regression, such as IP-IQA [Qu *et al.*, 2024], which predicts scores by fine-tuning feature extractors and training regression heads. However, they have key limitations: (1) insufficient exploitation of hierarchical and asymmetric entailment relations in image-text pairs. For instance, “Corgi” entails “dog” entails “animal”, but not vice versa. Simple symmetric Euclidean similarity struggles to capture such strict partial order relationships. Moreover, alignment scores containing rich fine-grained information are only used as regression targets without guiding geometric structure learning. (2) Existing methods typically employ unified mapping functions, ignoring the substantial complexity and characteristic variations across different samples. This one-size-fits-all approach leads to limited generalization when facing complex and diverse image-text pairs.

To address these issues, we propose HyperAlign, a T2IAA method based on hyperbolic entailment geometry. The core idea is to leverage the negative curvature property to explicitly model hierarchical entailment relations from text-to-image using entailment cone geometry in hyperbolic space. Specifically, HyperAlign first projects CLIP features onto the Lorentz hyperbolic manifold, where image-text relations are decoupled into three interpretable geometric features: exterior angle, entailment aperture, and hyperbolic distance. Then, by introducing ground-truth alignment scores as geo-

\*Corresponding author: gaoxb@cqupt.edu.cn



Figure 1: Illustration of the proposed geometric constraint mechanism.

metric constraint signals, as illustrated in Figure 1, we force high-alignment samples within narrower text cones while allowing low-alignment samples wider tolerance, transforming discrete entailment logic into continuous geometric supervision. Finally, we design an adaptive modulation regressor that generates sample-level modulation parameters from hyperbolic geometric features to adaptively calibrate Euclidean cosine similarity for alignment score prediction.

The main contributions of this work can be summarized as follows:

- We propose the first T2IAA method that incorporates hyperbolic entailment cones with a dynamic-supervision entailment modeling mechanism. This method overcomes Euclidean-space limitations in modeling asymmetric entailment relations, transforms abstract score regression into intuitive geometric constraint learning, and achieves deep coupling between alignment degree and spatial structure.
- We present an adaptive modulation regressor that utilizes entailment geometric features to generate sample-level modulation parameters, enabling personalized score mapping and improving generalization across complex and diverse samples.
- Extensive experiments on multiple mainstream AG-IQA benchmark datasets demonstrate that HyperAlign achieves highly competitive performance on both single-database and cross-database generalization tasks.

## 2 Related Work

### 2.1 Text-to-Image Alignment Assessment Methods

Traditional NS-IQA methods, although effective for measuring image distortion, fail to transfer effectively to AI-generated image scenarios. NS-IQA methods often assign high scores to pixel-level clear generated images, even if their content deviates from user-provided text descriptions.

To bridge this perceptual gap, assessment methods for generated images have gradually emerged. Early assessment methods like IS [Salimans *et al.*, 2016] and FID [Heusel *et al.*, 2017] measure overall distribution differences, but overlook image-text alignment. As generative paradigms evolved toward diffusion models, assessment focus has expanded beyond pixel-level distortions to incorporate semantic considerations, driving the emergence of AI-generated Image Quality Assessment (AG-IQA) methods. TIER [Yuan *et al.*, 2024] directly concatenates text and image features for quality score regression; IPCE [Peng *et al.*, 2024] transforms assessment into weighted classification probability by designing text templates with different matching degrees.

However, these methods often fail to effectively decouple visual quality and image-text alignment, or incorrectly equate alignment simply with overall quality. In fact, these are two relatively independent and even potentially conflicting dimensions: a visually realistic image may be completely irrelevant to the text, and vice versa. Addressing this issue, recent research attempts to isolate alignment as an independent assessment dimension. IP-IQA [Qu *et al.*, 2024] introduces Image2Prompt pre-training, using separate regression heads to predict quality and alignment respectively, achieving preliminary separation of assessment dimensions; Zhou *et al.* conducted in-depth exploration in this direction: they first proposed AMFF-Net [Zhou *et al.*, 2024], utilizing adaptive feature fusion modules to integrate multi-scale image features, configuring three independent regression heads for visual quality, realism, and alignment; subsequently, they further proposed CIA-Net [Zhou *et al.*, 2025], introducing cross-modal interactive attention modules that further enhanced joint prediction capability across these three dimensions through finer feature interaction. However, forcing simultaneous optimization of these two objectives within a shared-parameter encoder often leads to task interference. Furthermore, a greater limitation of these methods is the lack of explicit modeling of semantic hierarchical entailment relations, which results in limited generalization capability. Existing models primarily compute feature distances in Euclidean space, which essentially represents a flattened symmetric similarity metric. However, image-text correspondences are far more complex than simple similarity, with their core being directional asymmetric hierarchical entailment logic. This causes models to often ignore subtle image-text misalignments when facing complex fine-grained semantic combinations due to inability to distinguish hierarchical relations.

### 2.2 Hyperbolic Vision-Language Models

The negative curvature property of hyperbolic space enables low-distortion embedding of hierarchical structures. Compared to flat Euclidean space, hyperbolic space volume grows exponentially with radius. This advantage was first validated by Poincaré Embeddings [Nickel and Kiela, 2017] on the WordNet [Miller, 1995] hierarchy; subsequently, the Lorentz Model [Nickel and Kiela, 2018] improved numerical stability through Minkowski inner products.

Benefiting from excellent capabilities in representing hierarchical relations, hyperbolic geometry has been introduced

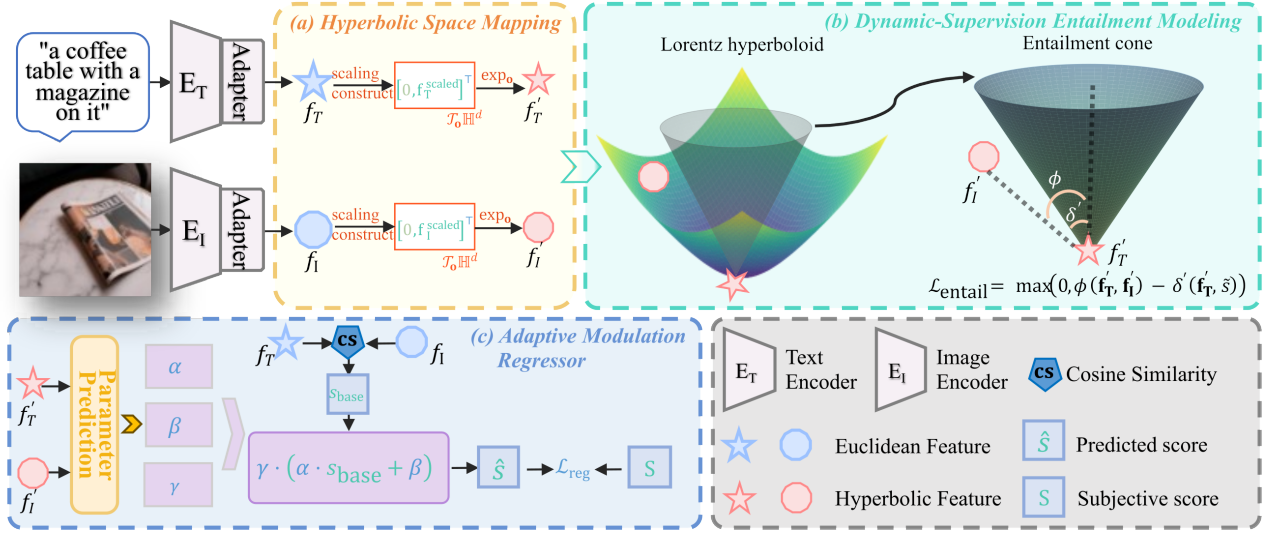


Figure 2: Overall architecture of HyperAlign.

to vision-language representation learning in recent years. MERU [Desai *et al.*, 2023] first elevated CLIP features to the Lorentz manifold, learning hierarchical representations by constraining text entails image partial order through entailment cones. HyCoCLIP [Pal *et al.*, 2025] optimized compositional entailment for complex scenes; HyperVLM [Srivastava and Wu, 2025] applied hyperbolic modeling to multimodal understanding. These works focus on pre-training and classification tasks, validating the effectiveness of hyperbolic space in modeling vision-language hierarchical relations. This paper explores its potential in fine-grained regression tasks by introducing a dynamic-supervision entailment modeling mechanism and adaptive modulation regressor, deeply integrating hyperbolic geometry with regression tasks, filling the gap in T2IAA, and effectively addressing the pain point that existing Euclidean space methods cannot precisely measure hierarchical semantic alignment.

### 3 Method

#### 3.1 Overall Framework

The overall architecture of HyperAlign is illustrated in Figure 2. For an input image-text pair  $(I, T)$ , we first extract original features using pre-trained CLIP model and introduce a lightweight gated Adapter based on [Gao *et al.*, 2024] to bridge the domain gap between pre-training and downstream tasks, obtaining Euclidean features  $f_I$  and  $f_T$ . We project them onto the Lorentz hyperbolic manifold through adaptive scaling, tangent vector construction, and exponential mapping, obtaining hyperbolic features  $f'_I$  and  $f'_T$ . We compute hyperbolic geometric features including hyperbolic distance, exterior angle, and entailment aperture, dynamically supervised by alignment scores to model finer-grained entailment hierarchical relations. Finally, we design an adaptive modulation regressor that utilizes extracted entailment geometric features to dynamically generate sample-level modulation parameters to calibrate Euclidean cosine similarity, effectively

combining the structural constraints of hyperbolic geometry with the semantic details of Euclidean space to output predicted score  $\hat{s}$ .

#### 3.2 Hyperbolic Space Mapping

Hyperbolic geometry features constant negative curvature, where space volume grows exponentially with radius, making it naturally suitable for modeling hierarchical structures. This subsection introduces the definition, metrics, and operations of hyperbolic space, along with the exponential mapping procedure for projecting Euclidean features onto the hyperbolic manifold.

**Lorentz Hyperbolic Manifold.** This paper adopts the Lorentz model to represent hyperbolic space. The Lorentz model  $\mathbb{H}^d$  of  $d$ -dimensional hyperbolic space is defined as the upper sheet of a double-sheeted hyperboloid in  $(d+1)$ -dimensional Minkowski spacetime:

$$\mathbb{H}^d = \{\mathbf{x} \in \mathbb{R}^{d+1} : \langle \mathbf{x}, \mathbf{x} \rangle_{\mathcal{L}} = -\frac{1}{c}, c > 0\}, \quad (1)$$

where  $c$  is the curvature parameter. For vector  $\mathbf{x} = [x_0, x_1, \dots, x_d]^T$ , following MERU's terminology, we call its first component  $x_0$  the time component, and the last  $d$  components  $\mathbf{x}_{\text{space}} = [x_1, \dots, x_d]^T \in \mathbb{R}^d$  the space components, satisfying  $x_0 = \sqrt{\frac{1}{c} + \|\mathbf{x}_{\text{space}}\|^2}$ .  $\langle \cdot, \cdot \rangle_{\mathcal{L}}$  is the Lorentzian inner product, defined as:

$$\langle \mathbf{x}, \mathbf{y} \rangle_{\mathcal{L}} = -x_0 y_0 + \sum_{i=1}^d x_i y_i. \quad (2)$$

The distance in the Lorentz model is induced by the Lorentz inner product, defined as:

$$d_{\mathcal{L}}(\mathbf{x}, \mathbf{y}) = \frac{1}{\sqrt{c}} \cdot \text{arccosh}(-c \langle \mathbf{x}, \mathbf{y} \rangle_{\mathcal{L}}). \quad (3)$$

The tangent space  $\mathcal{T}_{\mathbf{z}} \mathbb{H}^d$  is a  $d$ -dimensional Euclidean linear approximation of the manifold at point  $\mathbf{z}$ , consisting of

all vectors orthogonal to  $\mathbf{z}$  under the Lorentz inner product:  $\mathcal{T}_{\mathbf{z}}\mathbb{H}^d = \{\mathbf{v} \in \mathbb{R}^{d+1} : \langle \mathbf{z}, \mathbf{v} \rangle_{\mathcal{L}} = 0\}$ .

**Exponential Map.** We lift Euclidean space features from tangent space to hyperbolic manifold through exponential mapping. Generally, for point  $\mathbf{z} \in \mathbb{H}^d$  and vector  $\mathbf{v} \in \mathcal{T}_{\mathbf{z}}\mathbb{H}^d$  in its tangent space, the exponential map  $\exp_{\mathbf{z}} : \mathcal{T}_{\mathbf{z}}\mathbb{H}^d \rightarrow \mathbb{H}^d$  is defined as:

$$\exp_{\mathbf{z}}(\mathbf{v}) = \cosh(\sqrt{c}\|\mathbf{v}\|_{\mathcal{L}})\mathbf{z} + \frac{\sinh(\sqrt{c}\|\mathbf{v}\|_{\mathcal{L}})}{\sqrt{c}\|\mathbf{v}\|_{\mathcal{L}}}\mathbf{v}, \quad (4)$$

where  $\|\mathbf{v}\|_{\mathcal{L}} = \sqrt{|\langle \mathbf{v}, \mathbf{v} \rangle_{\mathcal{L}}|}$  is the hyperbolic norm.

In our implementation, to ensure numerical stability, we first perform adaptive scaling on Euclidean features  $\mathbf{f}$ :  $\mathbf{f}_{\text{scaled}} = \alpha \cdot \mathbf{f}$ , where  $\alpha = \sigma(\alpha_0) \cdot \alpha_{\max}$ ,  $\sigma(\cdot)$  is the sigmoid function,  $\alpha_0$  is a learnable parameter, and  $\alpha_{\max} = 1.0$  is the scaling upper bound. Then, using the origin of the hyperbolic space  $\mathbf{o} = [\sqrt{1/c}, 0, \dots, 0]^{\top}$  as the mapping base point, we construct tangent vector  $\mathbf{f} = [0, \mathbf{f}_{\text{scaled}}]^{\top} \in \mathcal{T}_{\mathbf{o}}\mathbb{H}^d$  in the origin tangent space, thus obtaining hyperbolic feature  $\mathbf{f}' = \exp_{\mathbf{o}}(\mathbf{f})$ .

Through these steps, the Euclidean image feature  $\mathbf{f}_I$  and text feature  $\mathbf{f}_T$  are respectively mapped to hyperbolic features  $\mathbf{f}'_I$  and  $\mathbf{f}'_T$ , laying the foundation for subsequent entailment relation modeling.

### 3.3 Dynamic-Supervision Entailment Modeling

Existing hyperbolic vision-language models typically only depend on text features to define entailment cones. These methods focus on whether entailment exists rather than capturing the degree of entailment, making them suitable for classification tasks but not directly applicable to continuous numerical regression tasks. For image-text alignment assessment, high-alignment samples should satisfy strict partial order relationships, while low-alignment samples should allow certain geometric deviations. To address this issue, we propose a dynamic-supervision mechanism with adaptive aperture that adjusts cone strictness based on alignment scores to construct fine-grained semantic hierarchies.

**Hyperbolic Entailment Geometric Primitives.** We decouple image-text relations into interpretable geometric features, enabling the model to understand from a geometric perspective whether text semantically contains the image. For hyperbolic embeddings  $\mathbf{f}'_T$  and  $\mathbf{f}'_I$ , the semantic range of text  $\mathbf{f}'_T$  is represented by an entailment cone with half-aperture angle  $\delta(\mathbf{f}'_T)$  that contracts as  $\mathbf{f}'_T$  moves away from the origin:

$$\delta(\mathbf{f}'_T) = \arcsin\left(\frac{2k}{\sqrt{c}\|\mathbf{f}'_{T,\text{space}}\|}\right), \quad (5)$$

where  $k$  is a constant controlling boundary conditions. This naturally encodes hierarchy: larger  $\|\mathbf{f}'_{T,\text{space}}\|$  yields narrower apertures that push aligned images outward, while general concepts near the origin maintain wide apertures accommodating diverse instances, making hyperbolic distance  $d_{\mathcal{L}}(\mathbf{o}, \cdot)$  a geometric proxy for semantic specificity. To measure image deviation, we compute exterior angle  $\phi(\mathbf{f}'_T, \mathbf{f}'_I)$  at vertex  $\mathbf{f}'_T$  in triangle  $\Delta O\mathbf{f}'_T\mathbf{f}'_I$ . By hyperbolic law of cosines with

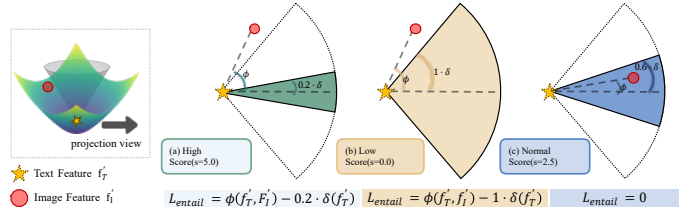


Figure 3: Visualization of dynamic-supervision entailment cones. High-alignment samples are constrained within narrow cones, while low-alignment samples are allowed wider cones.

$$\eta = \langle \mathbf{f}'_T, \mathbf{f}'_I \rangle_{\mathcal{L}}:$$

$$\phi(\mathbf{f}'_T, \mathbf{f}'_I) = \arccos\left(\frac{f'_{T,0} + f'_{T,0}c\eta}{\|\mathbf{f}'_{T,\text{space}}\| \sqrt{(c\eta)^2 - 1}}\right), \quad (6)$$

where  $f'_{T,0}, f'_{I,0}$  are time components,  $\mathbf{f}'_{T,\text{space}}$  are space components, and  $\langle \cdot, \cdot \rangle_{\mathcal{L}}$  is the Lorentzian inner product. Smaller  $\phi$  indicates stronger semantic alignment.

**Dynamic-Supervision Entailment Loss.** Rather than adopting a fixed entailment threshold, we innovatively introduce alignment scores as a geometric constraint signal. As illustrated in Figure 3, we design a dynamic adjustment mechanism that constrains high-alignment samples to fall within narrower text entailment cones, while allowing low-alignment samples wider cones, successfully transforming discrete entailment logic into continuous geometric structure supervision. We introduce modulation factor  $\gamma(\tilde{s})$  to adjust aperture based on ground-truth scores, where  $\tilde{s} \in [0, 1]$  is the normalized alignment score:

$$\gamma(\tilde{s}) = 1 - \alpha \cdot \tilde{s}, \quad \delta'(\mathbf{f}'_T, \tilde{s}) = \gamma(\tilde{s}) \cdot \delta(\mathbf{f}'_T), \quad (7)$$

where  $\alpha = 0.8$  controls maximum contraction. Higher alignment scores yield smaller  $\gamma(\tilde{s})$ , producing narrower cones. The dynamic-supervision entailment loss is:

$$\mathcal{L}_{\text{entail}}(\mathbf{f}'_T, \mathbf{f}'_I, \tilde{s}) = \max(0, \phi(\mathbf{f}'_T, \mathbf{f}'_I) - \delta'(\mathbf{f}'_T, \tilde{s})). \quad (8)$$

By minimizing this loss, high-alignment samples are constrained within tight cones, while low-alignment samples receive relaxed constraints, enabling the model to learn not only partial order relationships but also encode alignment scores into the hierarchical geometric structure. Since text embeddings gravitate toward the origin while strictly aligned images are pushed outward, this establishes a distance-based hierarchical representation.

### 3.4 Adaptive Modulation Regressor

Although hyperbolic space can precisely characterize hierarchical entailment relations between text and images, the exponential mapping with numerical stability constraints may not fully preserve the rich semantic priors accumulated by pre-trained models in Euclidean space. Additionally, hyperbolic metrics are extremely sensitive to numerical values, making them unsuitable for direct score regression. Therefore, this paper proposes an adaptive modulation regressor with the core idea: retain Euclidean cosine similarity as the base metric, using hyperbolic entailment geometric features

---

**Algorithm 1** Adaptive Modulation Regressor

---

**Require:** Euclidean features  $\mathbf{f}_I, \mathbf{f}_T$ ; Hyperbolic primitives  $\mathcal{Z} = \{d_{\mathcal{L}}, \phi, \delta\}$   
**Ensure:** Predicted alignment score  $\hat{s}$   
1:  $s_{\text{base}} \leftarrow \text{CosineSimilarity}(\mathbf{f}_I, \mathbf{f}_T)$   
2:  $\alpha, \beta, \gamma \leftarrow \mathcal{M}(\mathcal{Z})$   
3:  $\hat{s} \leftarrow \gamma \cdot (\alpha \cdot s_{\text{base}} + \beta)$   
4: **return**  $\hat{s}$

---

to dynamically modulate cosine similarity, thereby achieving complementary advantages of both geometric spaces. We design a lightweight parameter prediction network, ModulationNet, which does not directly output scores but rather observes geometric primitives in hyperbolic space: hyperbolic distance  $d_{\mathcal{L}}$ , exterior angle  $\phi$ , and aperture  $\delta$ , thereby perceiving the current structural alignment state and generating a set of modulation parameters accordingly. This design cleverly fuses the structural sensitivity of hyperbolic space with the numerical stability of Euclidean space. For samples with perfect entailment relations, the model enhances their confidence; for samples at entailment boundaries or violating hierarchy, geometric features guide the model to penalize base semantic scores. The logic flow of this method is shown in Algorithm 1. The mapping function  $\mathcal{M}$  generates three parameters with clear physical meaning: Scale ( $\alpha$ ) adjusts the dynamic range of cosine similarity, amplifying the discriminability of high-alignment samples. Bias ( $\beta$ ) corrects systematic biases, such as compensation when images are semantically correct but positioned at the edge in hyperbolic space. Confidence ( $\gamma$ ) acts as a gating mechanism, reducing the contribution weight of samples with highly uncertain geometric structures to the final score.

HyperAlign’s training is jointly driven by regression accuracy and geometric structure constraints. The total loss function  $\mathcal{L}_{\text{total}}$  is defined as:

$$\mathcal{L}_{\text{total}} = \mathcal{L}_{\text{reg}} + \lambda \cdot \mathcal{L}_{\text{entail}}, \quad (9)$$

where  $\lambda$  is a weight coefficient, and  $\mathcal{L}_{\text{reg}}$  adopts L1 loss to minimize the absolute error between predicted score  $\hat{s}$  and human ratings.

## 4 Experiments

### 4.1 Experimental Setup

**Datasets.** We conduct evaluations on three mainstream benchmark datasets. **AGIQA-3K** [Li *et al.*, 2023] comprises 2982 AI-generated images from six generative models, covering diverse prompt types including objects, scenes, and styles, with human-annotated alignment Mean Opinion Scores (MOS) ranging from 1 to 5. **AIGCIQA2023** [Wang *et al.*, 2023b] consists of 2400 images generated by eight mainstream models, with prompts spanning multiple topic categories and alignment MOS ranging from 1 to 5. **PKU-I2IQA** [Yuan *et al.*, 2023] contains 2000 image pairs with alignment MOS ranging from 1 to 5. For single-database evaluation, following previous works, we use 4:1 train-test splits for AGIQA-3K and AIGCIQA2023, 3:1 splits for PKU-I2IQA, ensuring identical text prompts appear only within the

same subset to prevent content overlap. We report average results over ten random splits.

**Evaluation Metrics.** We use two widely adopted metrics: Spearman Rank Correlation Coefficient (SRCC) and Pearson Linear Correlation Coefficient (PLCC). The SRCC measures the monotonic relationship between predicted and ground-truth scores, robust to outliers. The PLCC measures the linear goodness-of-fit between predicted and true values, more sensitive to absolute prediction accuracy. Both range from -1 to 1, with values closer to 1 indicating better model performance.

**Implementation Details.** We use ViT-B/16 CLIP with batch size 8 and AdamW optimizer, adopting grouped learning rates: CLIP backbone  $2 \times 10^{-6}$  with weight decay  $1 \times 10^{-4}$ , Adapter and regressor  $4 \times 10^{-4}$  with weight decay 0.005. Learning rate scheduling uses StepLR strategy, decaying to 0.5 of the original every 10 epochs. L1 loss with entailment loss weight  $\lambda = 0.1$ . Training employs mixed-precision to accelerate computation, with maximum epochs set to 20 and early stopping strategy that terminates training when validation set SRCC does not improve for 6 consecutive epochs. All experiments are conducted on a single NVIDIA GeForce GTX4090 GPU.

### 4.2 Single Database Performance Evaluation

Following the experimental setup described above, we validate HyperAlign’s effectiveness on T2IAA by comparing against 12 mainstream methods, including 8 NS-IQA and 4 AG-IQA methods. As shown in Table 1, the results reveal a substantial performance gap between traditional NS-IQA and AG-IQA methods, confirming that single-modality methods face significant challenges when directly applied to generative assessment. In contrast, HyperAlign achieves state-of-the-art performance across all datasets with an average SRCC of 0.8190, surpassing the second-best method CIA-Net by 1.99 percentage points. HyperAlign’s superior performance is fundamentally attributed to the synergistic effect of hyperbolic entailment modeling and adaptive modulation regression. Specifically, hyperbolic space’s hierarchical modeling capability enables HyperAlign to capture asymmetric entailment relations across different semantic levels, explicitly encoding whether generated images satisfy the hierarchical containment logic required by text prompts. Building upon this geometric foundation, the adaptive modulation regressor further leverages entailment geometric features to generate sample-level calibration parameters, enabling personalized score mapping that effectively captures fine-grained alignment characteristics between diverse image content and text prompts. By tightly coupling geometric structure constraints with adaptive score calibration, HyperAlign achieves significant performance gains across all benchmarks.

### 4.3 Ablation Studies

To deeply analyze the contribution of each component of HyperAlign, we design a series of ablation experiments. Using the same configuration as the single-database evaluation, we conduct 10 repeated experiments and report the average results. Specifically, we mainly examine the following three key components: 1) static entailment cone (without dynamic

Table 1: Single database performance comparison. Best results are in **bold**, second-best are underlined.

Method	Venue	AGIQA-3K		AIGCIQA2023		PKU-I2IQA		Avg.
		SRCC	PLCC	SRCC	PLCC	SRCC	PLCC	
DB-CNN [Zhang <i>et al.</i> , 2020]	TCSVT’20	0.6329	0.7823	0.6837	0.6787	0.6083	0.5925	0.6631
HyperIQA [Su <i>et al.</i> , 2020]	CVPR’20	0.6276	0.8087	0.7541	0.7439	0.7239	0.7062	0.7274
MUSIQ [Ke <i>et al.</i> , 2021]	ICCV’21	0.6292	0.7839	0.7620	0.7527	0.6379	0.6531	0.7031
TReS [Golestaneh <i>et al.</i> , 2022]	TIP’22	0.6366	0.8134	0.7292	0.7266	0.6480	0.6456	0.6999
Re-IQA [Saha <i>et al.</i> , 2023]	CVPR’23	0.6373	0.7880	0.6430	0.6355	0.5705	0.5690	0.6406
StairIQA [Sun <i>et al.</i> , 2023]	JSTSP’23	0.6348	0.8006	0.6641	0.6625	0.5739	0.5720	0.6513
LIQE [Zhang <i>et al.</i> , 2023]	CVPR’23	0.6516	0.7404	0.7705	0.7589	0.7627	0.7115	0.7326
CLIPiQA [Wang <i>et al.</i> , 2023a]	AAAI’23	0.6456	0.6607	0.7321	0.6826	0.7071	0.6148	0.6738
IP-IQA [Qu <i>et al.</i> , 2024]	ICME’24	0.7578	0.8544	-	-	-	-	-
AMFF-Net [Zhou <i>et al.</i> , 2024]	TBC’24	0.7513	0.8476	0.7782	0.7638	0.7796	0.7708	0.7819
IPCE [Peng <i>et al.</i> , 2024]	CVPRW’24	0.7697	<u>0.8725</u>	<u>0.7979</u>	<u>0.7887</u>	-	-	-
CIA-Net [Zhou <i>et al.</i> , 2025]	PR’25	<u>0.7797</u>	0.8687	0.7977	0.7800	0.7855	<u>0.7829</u>	<u>0.7991</u>
HyperAlign (ours)	-	<b>0.7927</b>	<b>0.8830</b>	<b>0.8078</b>	<b>0.8013</b>	<b>0.7977</b>	<b>0.8316</b>	<b>0.8190</b>

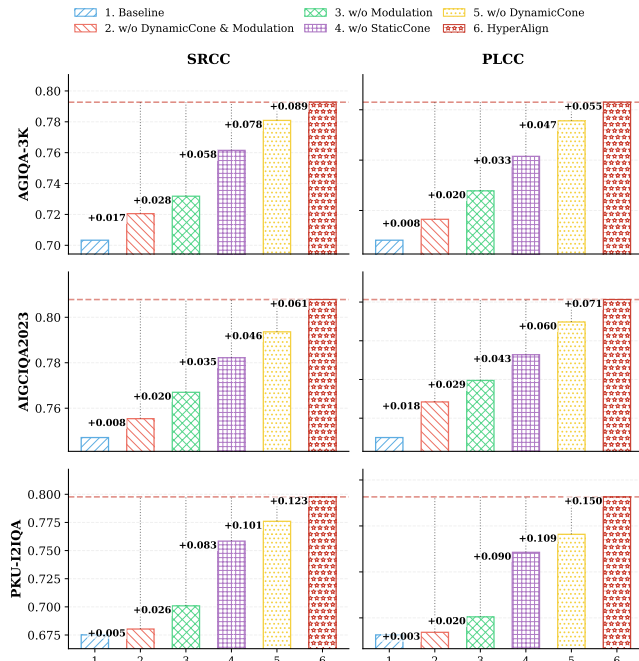


Figure 4: Ablation study of HyperAlign on three standard datasets.

supervision), 2) dynamic-supervision entailment cone, and 3) adaptive modulation regressor.

Figure 4 reveals a progressive performance trend across six configurations. The bar charts demonstrate that entailment cone modeling alone yields some gains: configuration (2) with static cone achieves +0.017/+0.008 on AGIQA-3K/AIGCIQA2023, while (3) with dynamic-supervision cone reaches +0.028/+0.020, showing improvements over baseline (1). This indicates that while explicit entailment constraints do bring certain performance improvements, the hyperbolic hierarchical structures cannot be effectively exploited without adaptive modulation. Remarkably, configuration (4), using Modulation without any entailment cone, achieves dra-

matic jumps of +0.058, +0.035, and +0.083 across datasets. This may be attributed to two factors: the latent hierarchical semantics already present in CLIP features after hyperbolic projection, and the positive effects brought by sample-level adaptive parameters that enable personalized score mapping. Meanwhile, comparing (3) to (2) confirms that the dynamic-supervision cone’s adaptive aperture outperforms the static cone’s fixed geometry even without modulation. The synergistic effect becomes evident in configurations (5) and (6): reintroducing entailment cones atop modulation yields substantial additional gains. Configuration (5) with static cone reaches +0.078/+0.046/+0.101, while the full HyperAlign (6) with dynamic-supervision cone achieves peak improvements of +0.089/+0.061/+0.123. Notably, the dynamic-supervision cone consistently outperforms the static cone both without modulation (comparing 2 vs 3: +0.011/+0.012) and with modulation (comparing 5 vs 6: +0.011/+0.015/+0.022), confirming its superiority. These results demonstrate that explicit geometric supervision and feature-guided modulation complement each other, jointly establishing an optimal hierarchical structure for alignment assessment.

#### 4.4 Visualization Analysis

To intuitively demonstrate the improvement effect of hyperbolic space mapping on feature representation, we conduct image feature space visualization experiments on the AIGCIQA2023 dataset. We focus on visualizing image features because they directly reflect how the model organizes visual concepts according to their alignment degrees with prompts, providing clearer insights into the learned hierarchical structure. Specifically, we compare three types of image feature representations: 1) CLIP original features with directly loaded pre-trained weights without downstream task training, 2) trained Euclidean features fine-tuned on the downstream alignment assessment task, and 3) trained hyperbolic features fine-tuned on the downstream alignment assessment task. For Euclidean features, we apply t-SNE for dimensionality reduction; for hyperbolic features, we apply CO-SNE [Guo *et al.*, 2022], which preserves distances and more accurately maintains hyperbolic geometric structure.

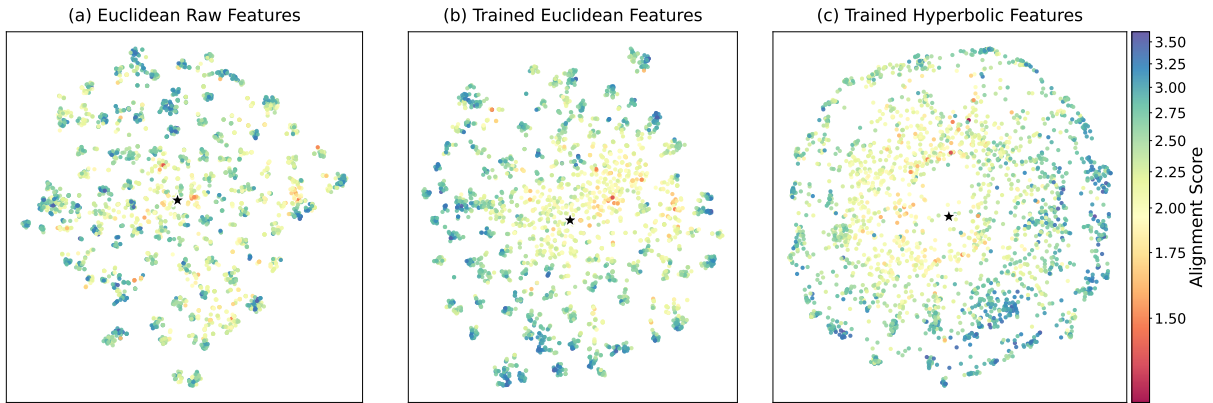


Figure 5: Feature space visualization on AIGCIQA2023 dataset using t-SNE for Euclidean features and CO-SNE for hyperbolic features.

Table 2: Comparison of results on cross-database testing. Best results are in **bold**, second-best are underlined.

Method	AIGCIQA2023		AGIQA3K → AIGCIQA2023		Avg.
	SRCC	PLCC	SRCC	PLCC	
DB-CNN	0.3900	0.4350	0.4700	0.4600	0.4388
HyperIQA	0.4180	0.4650	0.4640	0.4310	0.4445
MUSIQ	0.3940	0.4370	0.5250	0.5150	0.4678
TRES	0.4450	0.4880	0.5050	0.4830	0.4803
Re-IQA	0.2430	0.1540	0.4790	0.4840	0.3400
LIQE	0.5002	0.4830	0.4927	0.5188	0.4987
CLIPQA	0.4809	0.4409	0.4300	0.4400	0.4480
AMFF-Net	<u>0.5537</u>	<u>0.6240</u>	0.5461	0.5485	0.5681
CIA-Net	0.5287	0.5498	<b>0.6506</b>	<b>0.7443</b>	<u>0.6184</u>
<b>Ours</b>	<b>0.7013</b>	<b>0.7926</b>	<u>0.6309</u>	<u>0.6244</u>	<b>0.6873</b>

As shown in Figure 5, CLIP original features demonstrate certain clustering capability but lack hierarchical stratification across different score levels. Trained Euclidean features show improved separation with emerging hierarchical tendencies, yet the stratification remains subtle with considerable overlap among score groups. In contrast, trained hyperbolic features reveal pronounced radial hierarchical structure: low-score samples in warm colors concentrate near the origin, while high-score samples in cool colors disperse toward the disk boundary, forming distinct hierarchical layers. This aligns with hyperbolic geometric properties where distance from the origin encodes semantic specificity—nodes farther from the origin with larger norms correspond to leaf-level specific concepts, while those near the origin represent abstract concepts. This visualization geometrically validates the effectiveness of entailment loss and feature guidance in HyperAlign, demonstrating that hyperbolic space naturally provides an ideal geometric foundation for hierarchical alignment modeling.

#### 4.5 Cross Database Performance Evaluation

To evaluate HyperAlign’s generalization capability, we conduct cross-database experiments by training on one dataset and testing on another. Specifically, we examine two sce-

narios: 1) training on AIGCIQA2023 and testing on AGIQA-3K; 2) training on AGIQA-3K and testing on AIGCIQA2023. PKU-I2IQA is excluded as it involves image-to-image rather than text-to-image generation. Each experiment is repeated with different random seeds and we report the average results. Table 2 presents cross-database generalization results, revealing that all methods exhibit significantly degraded performance compared to single database evaluation, reflecting the challenge of domain shift. HyperAlign achieves an average SRCC of **0.6873**, outperforming the second-best method CIA-Net (0.6184) by 6.89 percentage points, demonstrating superior cross-database generalization. This robustness is primarily attributed to hyperbolic entailment modeling: entailment relations are encoded through conical geometric constraints in hyperbolic space, which capture fundamental semantic hierarchies independent of dataset-specific distribution characteristics, thereby ensuring strong transferability. The entailment feature guidance mechanism leverages geometric primitives to enhance representations based on intrinsic relational structures rather than data-driven statistical patterns, making them inherently robust to distribution shifts. This experiment validates the model’s generalization capability.

## 5 Conclusion

This paper has proposed HyperAlign, an image-text alignment assessment framework based on hyperbolic space, utilizing hyperbolic geometry to model the hierarchical entailment relations between images and text. By designing a dynamic-supervision entailment modeling mechanism in hyperbolic space, we have effectively captured the hierarchical semantic structures inherent in image-text pairs. Ablation experiments have validated the synergistic effect of entailment loss and entailment feature guidance, indicating that both components complementarily promote performance improvement. Extensive experiments on three AIGC assessment benchmarks have demonstrated that HyperAlign outperforms existing methods. In the future, we will explore integrating large language models into our method to develop alignment assessment methods with more interpretable outputs.

## References

[Desai *et al.*, 2023] Karan Desai, Maximilian Nickel, Tanmay Rajpurohit, Justin Johnson, and Shanmukha Ramakrishna Vedantam. Hyperbolic image-text representations. In *Proceedings of the International Conference on Machine Learning (ICML)*, pages 7694–7731, 2023.

[Gao *et al.*, 2024] Peng Gao, Shijie Geng, Renrui Zhang, Teli Ma, Rongyao Fang, Yongfeng Zhang, Hongsheng Li, and Yu Qiao. Clip-adapter: Better vision-language models with feature adapters. *International Journal of Computer Vision*, 132(2):581–595, 2024.

[Golestaneh *et al.*, 2022] S Alireza Golestaneh, Saba Dadsetan, and Kris M Kitani. No-reference image quality assessment via transformers, relative ranking, and self-consistency. In *Proceedings of the IEEE/CVF Winter Conference on Applications of Computer Vision (WACV)*, pages 1220–1230, 2022.

[Guo *et al.*, 2022] Yunhui Guo, Haoran Guo, and Stella X Yu. Co-sne: Dimensionality reduction and visualization for hyperbolic data. In *Proceedings of the IEEE/CVF Conference on Computer Vision and Pattern Recognition (CVPR)*, pages 21–30, 2022.

[Heusel *et al.*, 2017] Martin Heusel, Hubert Ramsauer, Thomas Unterthiner, Bernhard Nessler, and Sepp Hochreiter. Gans trained by a two time-scale update rule converge to a local nash equilibrium. In *Proceedings of the Advances in Neural Information Processing Systems (NeurIPS)*, volume 30, 2017.

[Hu *et al.*, 2025] Zijing Hu, Fengda Zhang, Long Chen, Kun Kuang, Jiahui Li, Kaifeng Gao, Jun Xiao, Xin Wang, and Wenwu Zhu. Towards better alignment: Training diffusion models with reinforcement learning against sparse rewards. In *Proceedings of the IEEE/CVF Conference on Computer Vision and Pattern Recognition (CVPR)*, pages 23604–23614, 2025.

[Ke *et al.*, 2021] Junjie Ke, Qifei Wang, Yilin Wang, Peyman Milanfar, and Feng Yang. Musiq: Multi-scale image quality transformer. In *Proceedings of the IEEE/CVF International Conference on Computer Vision (ICCV)*, pages 5148–5157, 2021.

[Li *et al.*, 2023] Chunyi Li, Zicheng Zhang, Haoning Wu, Wei Sun, Xiongkuo Min, Xiaohong Liu, Guangtao Zhai, and Weisi Lin. Agiqa-3k: An open database for ai-generated image quality assessment. *IEEE Transactions on Circuits and Systems for Video Technology*, 34(8):6833–6846, 2023.

[Miller, 1995] George A. Miller. Wordnet: A lexical database for english. *Communications of the ACM*, 38(11):39–41, 1995.

[Mittal *et al.*, 2012] Anish Mittal, Anush Krishna Moorthy, and Alan Conrad Bovik. No-reference image quality assessment in the spatial domain. *IEEE Transactions on Image Processing (TIP)*, 21(12):4695–4708, 2012.

[Mittal *et al.*, 2013] Anish Mittal, Rajiv Soundararajan, and Alan C Bovik. Making a “completely blind” image quality analyzer. *IEEE Signal Processing Letters*, 20(3):209–212, 2013.

[Nickel and Kiela, 2017] Maximilian Nickel and Douwe Kiela. Poincaré embeddings for learning hierarchical representations. In *Proceedings of the Advances in Neural Information Processing Systems (NeurIPS)*, volume 30, 2017.

[Nickel and Kiela, 2018] Maximilian Nickel and Douwe Kiela. Learning continuous hierarchies in the lorentz model of hyperbolic geometry. In *Proceedings of the International Conference on Machine Learning (ICML)*, volume 80, pages 3779–3788, 2018.

[Pal *et al.*, 2025] Avik Pal, Max van Spengler, Guido Maria D’Amely di Melendugno, Alessandro Flaboreo, Fabio Galasso, and Pascal Mettes. Compositional entailment learning for hyperbolic vision-language models. In *Proceedings of the Thirteenth International Conference on Learning Representations (ICLR)*, 2025.

[Peng *et al.*, 2024] Fei Peng, Huiyuan Fu, Anlong Ming, Chuanming Wang, Huadong Ma, Shuai He, Zifei Dou, and Shu Chen. Aigc image quality assessment via image-prompt correspondence. In *Proceedings of the IEEE/CVF Conference on Computer Vision and Pattern Recognition*, pages 6432–6441, 2024.

[Qu *et al.*, 2024] Bowen Qu, Haohui Li, and Wei Gao. Bringing textual prompt to ai-generated image quality assessment. In *Proceedings of the 2024 IEEE International Conference on Multimedia and Expo (ICME)*, pages 1–6, 2024.

[Radford *et al.*, 2021] Alec Radford, Jong Wook Kim, Chris Hallacy, Aditya Ramesh, Gabriel Goh, Sandhini Agarwal, Girish Sastry, Amanda Askell, Pamela Mishkin, Jack Clark, et al. Learning transferable visual models from natural language supervision. In *Proceedings of the International Conference on Machine Learning (ICML)*, pages 8748–8763, 2021.

[Ramesh *et al.*, 2021] Aditya Ramesh, Mikhail Pavlov, Gabriel Goh, Scott Gray, Chelsea Voss, Alec Radford, Mark Chen, and Ilya Sutskever. Zero-shot text-to-image generation. In *Proceedings of the International Conference on Machine Learning (ICML)*, pages 8821–8831, 2021.

[Rombach *et al.*, 2022] Robin Rombach, Andreas Blattmann, Dominik Lorenz, Patrick Esser, and Björn Ommer. High-resolution image synthesis with latent diffusion models. In *Proceedings of the IEEE/CVF Conference on Computer Vision and Pattern Recognition (CVPR)*, pages 10684–10695, 2022.

[Saha *et al.*, 2023] Avinab Saha, Sandeep Mishra, and Alan C Bovik. Re-iqa: Unsupervised learning for image quality assessment in the wild. In *Proceedings of the IEEE/CVF Conference on Computer Vision and Pattern Recognition (CVPR)*, pages 5846–5855, 2023.

[Salimans *et al.*, 2016] Tim Salimans, Ian Goodfellow, Wojciech Zaremba, Vicki Cheung, Alec Radford, and Xi Chen.

Improved techniques for training gans. In *Proceedings of the Advances in Neural Information Processing Systems (NeurIPS)*, volume 29, 2016.

[Srivastava and Wu, 2025] Sarthak Srivastava and Kathy Wu. Hypervlm: Hyperbolic space guided vision language modeling for hierarchical multi-modal understanding. In *Proceedings of the IEEE/CVF International Conference on Computer Vision (ICCV)*, pages 2347–2358, 2025.

[Su *et al.*, 2020] Shaolin Su, Qingsen Yan, Yu Zhu, Cheng Zhang, Xin Ge, Jinqiu Sun, and Yanning Zhang. Blindly assess image quality in the wild guided by a self-adaptive hyper network. In *Proceedings of the IEEE/CVF Conference on Computer Vision and Pattern Recognition (CVPR)*, pages 3667–3676, 2020.

[Sun *et al.*, 2023] Wei Sun, Xiongkuo Min, Danyang Tu, Siwei Ma, and Guangtao Zhai. Blind quality assessment for in-the-wild images via hierarchical feature fusion and iterative mixed database training. *IEEE Journal of Selected Topics in Signal Processing*, 2023.

[Wang *et al.*, 2023a] Jianyi Wang, Kelvin CK Chan, and Chen Change Loy. Exploring clip for assessing the look and feel of images. In *Proceedings of the AAAI Conference on Artificial Intelligence (AAAI)*, volume 37, pages 2555–2563, 2023.

[Wang *et al.*, 2023b] Jiarui Wang, Huiyu Duan, Jing Liu, Shi Chen, Xiongkuo Min, and Guangtao Zhai. Aigcqa2023: A large-scale image quality assessment database for ai generated images: from the perspectives of quality, authenticity and correspondence. In *Proceedings of the CAAI International Conference on Artificial Intelligence (CIAI)*, pages 46–57, 2023.

[Yuan *et al.*, 2023] Jiquan Yuan, Xinyan Cao, Changjin Li, Fanyi Yang, Jinlong Lin, and Xixin Cao. Pku-i2iqa: An image-to-image quality assessment database for ai generated images. *arXiv preprint arXiv:2311.15556*, 2023.

[Yuan *et al.*, 2024] Jiquan Yuan, Xinyan Cao, Changjie Fan, and Zhentao Liu. Tier: Text-image encoder-based regression for aigc image quality assessment. *arXiv preprint arXiv:2401.03854*, 2024.

[Zhang *et al.*, 2020] Weixia Zhang, Kede Ma, Jia Yan, Dexiang Deng, and Zhou Wang. Blind image quality assessment using a deep bilinear convolutional neural network. *IEEE Transactions on Circuits and Systems for Video Technology*, 30(1):36–47, 2020.

[Zhang *et al.*, 2023] Weixia Zhang, Guangtao Zhai, Ying Wei, Xiaokang Yang, and Kede Ma. Blind image quality assessment via vision-language correspondence: A multi-task learning perspective. In *Proceedings of the IEEE/CVF Conference on Computer Vision and Pattern Recognition (CVPR)*, pages 14071–14081, 2023.

[Zhou *et al.*, 2024] Tianwei Zhou, Songbai Tan, Wei Zhou, Yu Luo, Yuan-Gen Wang, and Guanghui Yue. Adaptive mixed-scale feature fusion network for blind ai-generated image quality assessment. *IEEE Transactions on Broadcasting*, 70(3):833–843, 2024.

[Zhou *et al.*, 2025] Tianwei Zhou, Songbai Tan, Leida Li, Baoquan Zhao, Qiuping Jiang, and Guanghui Yue. Cross-modality interactive attention network for ai-generated image quality assessment. *Pattern Recognition*, page 111693, 2025.